

# Bamboo-Based Activated Carbon @ MnO<sub>2</sub> Nanocomposites for Flexible High-Performance Supercapacitor Electrode Materials

Tianfu Huang, Zehai Qiu, Dewu Wu, Zhibiao Hu\*

College of Chemistry & Materials Science, LongYan University, FuJianLongYan, 364012, China

\*E-mail: [hhtff@126.com](mailto:hhtff@126.com)

Received: 25 April 2015 / Accepted: 19 May 2015 / Published: 24 June 2015

---

Porous nano-MnO<sub>2</sub> decorated bamboo-based activated carbon was fabricated by an *in situ* preparation method. MnO<sub>2</sub> with size of about 16.92 nm is uniformly loaded on the surface of bamboo-based activated carbon. Such unique bamboo-based activated carbon @ MnO<sub>2</sub> nanocomposites exhibited excellent electrochemical performance: a high specific capacitance of 221.45 F g<sup>-1</sup> at the current density of 1 A g<sup>-1</sup>, an excellent rate capability and a good cycling performance with 89.29% retention after 1000 cycles at the current density of 1 A g<sup>-1</sup>. The results indicate that this kind of hybrid core-shell bamboo-based activated carbon @ MnO<sub>2</sub> nanocomposites have great potential in future practical applications.

---

**Keywords:** bamboo-based activated carbon; MnO<sub>2</sub>; supercapacitor

## 1. INTRODUCTION

To address the rapid depletion of fossil fuels and environmental pollution issues, there is an urgent demand to develop renewable and clean energy sources [1]. Electrochemical capacitors (also called supercapacitors) have attracted increasing interests over the past few years due to their high specific capacitance, high power density, and long cyclic stability. Electrochemical capacitors store energy primarily by utilizing the electrical double layer (EDL) and redox reactions (pseudo-capacitance), which provide high power and long cycle life but lower energy as compared to rechargeable batteries [2]. Therefore, the choice of suitable active electrode materials for supercapacitors to meet the requirements of high energy and power is a promising field of research. Various active materials which have been studied include carbon based materials, transition metal oxides, conductive polymers [3-6]. Each of them has its own advantages and disadvantages. Carbon materials have outstanding electrical properties, long life-cycles and great mechanical properties, but

small double layer capacitance. Conducting polymers are inexpensive and flexible, but have poor cyclability. Transition metal oxide materials have high specific capacitance, but they are expensive. Therefore, binary or ternary composites have been extensively synthesized and investigated with the goal of obtaining materials with a combined and balanced merit of the three kind materials [7].

It has been demonstrated that the construction of carbon-inorganic composite is an effective strategy to improve the electrochemical utilization of metal oxides and carbon materials [8, 9]. For instance, K. J. Huang's group [10] prepared hierarchical-structured copper sulfide/multi-walled carbon nanotubes using a one-step hydrothermal process, and it was found that the nanocomposites exhibited a much higher specific capacitance up to  $2831 \text{ F g}^{-1}$ , compared with  $925.1 \text{ F g}^{-1}$  for CuS and  $555.6 \text{ F g}^{-1}$  for MWCNT. Ty Mai Dinh's group [11] demonstrated the fabrication of vertically aligned carbon nanowalls decorated with porous ruthenium oxide as a high-performance electrode for all-solid-state micro-supercapacitors, which deliver specific capacitance in excess of  $100 \text{ mF cm}^{-2}$  and energy density comparable to that of lithiumion micro-batteries, and are superior power and cycling stability. Transition metal oxides such as NiO [12], RuO<sub>2</sub> [13], Co<sub>3</sub>O<sub>4</sub> [14] and MnO<sub>2</sub> [15] are widely used as pseudocapacitors ( PDCs ). Among them, RuO<sub>2</sub> and MnO<sub>2</sub> are ideal candidate materials for pseudocapacitors because of their variable oxidation states, good chemical and electrochemical stability, easy preparation and high theoretical specific capacitances. However, low porosity, high cost and toxic nature of RuO<sub>2</sub> limit its commercialization in supercapacitors. In comparison, MnO<sub>2</sub> is currently considered as one of the most promising redox components for supercapacitor application owing to its natural abundance, cheap, environmental friendliness and high capacitance [16, 17]. To date, various MnO<sub>2</sub>/carbon composites have been synthesized and used as supercapacitor materials, such as composites with ordered mesoporous carbon [18], graphene [19], carbon nanotubes [20], nanofoam [21] and carbon aerogels [22]. Indeed, the electrochemical capacitance of these composites can be significantly improved. Especially, carbon nanotubes ( CNTs ) and graphene are welcomed candidates for MnO<sub>2</sub>/carbon composites. However, these are man-made carbon substrates, whose manufacturing processes are extremely complex and whose manufacturing costs are very expensive. Thus, man-made carbon substrates are limited to application in industry. It is necessary and urgent to look for new substitutes for carbon substrates.

Bamboo-based activated carbon is one of important carbon substrates in nature. It is made of bamboo, which is widely distributed in the world, grows fast, and whose output is big. Moreover, bamboo-based activated carbon has an extraordinarily porous 3D microstructure and high absorptive capacity. The porous 3D microstructure of bamboo is suitable for both absorption and desorption of electrolyte ions without chemical reactions, and high conductive properties enable to complete the rapid charging [23]. Therefore, bamboo-based activated carbon is one of the best carbon substrate for preparation of MnO<sub>2</sub>/carbon composites due to its low cost and abundant raw materials.

Herein, we presented a facile, efficient and low-cost preparation of bamboo-based activated carbon @ MnO<sub>2</sub> core-shell nanocomposites as the electrode materials for supercapacitors with improved electrochemical performances. The MnO<sub>2</sub> nanoshells can be in situ anchored on surfaces of the bamboo-based activated carbon through a facile redox reaction between KMnO<sub>4</sub> and carbon. By adjusting the reaction time, we can easily control the structure, composition of the MnO<sub>2</sub> and interfaces of the composites. The structure, morphology and electrochemical properties of as-prepared

nanocomposites were investigated. Remarkably, the as-prepared nanocomposites exhibited promising specific capacitance, excellent rate ability, and good cycle stability for supercapacitor applications. Therefore, the abundant natural bamboo could be an excellent activated carbon electrode, replacing expensive man-made carbon substrates, for energy storage devices.

## 2. EXPERIMENTAL

### 2.1 Synthesis of bamboo-based activated carbon @ MnO<sub>2</sub> nanocomposites

All of the chemical reagents were analytical purity and used without any further purification. Typical bamboo-based activated carbon was purchased from Fujian Longyan Longneng Flyash Comprehensive Utilization Co., Ltd, China. The commercial bamboo-based activated carbon was firstly washed with deionized water to remove dust and then placed in a mixer at 20,000 rpm for 3 min to make a fine powder. Then powder was treated with 3 M HCl for 12 h to remove any residue of organic contamination. The treated bamboo-based activated carbon powder was filtered by the vacuum filtration ( 0.45 μm of nylon filter paper ) with deionized water several times and anhydrous ethanol three times, finally dried for 12 h in a vacuum oven.

The synthesis of bamboo-based activated carbon @ MnO<sub>2</sub> nanocomposites was based on the redox reaction [16] as below:



Firstly, 0.36 g of bamboo-based activated carbon powder and 6.3212 g of KMnO<sub>4</sub> were dispersed in 100 mL of aqueous solution under high- power ultrasonications for 0.5 h. Secondly, 60 mL of the freshly obtained suspension liquid was added into a 80-mL Teflon-sealed autoclave and maintained at 100 °C for different time ( 60, 90, 120 min ). To prevent the products from aggregating and precipitating, a small stirring rotor was put into the autoclave beforehand and the heating process was completed in an oil-bath heating apparatus with a magnetic string system. After the specified reaction time, the autoclave was picked out, immediately put into a pool with flowing cooling water and stayed for several minutes to be cooled down to the room temperature. Thirdly, the products were isolated by centrifugation at a rate of 12,000 r min<sup>-1</sup>, and then cleaned by five centrifugation / washing / re-dispersion cycles in water and dried at 100 °C for 6 h in air. Finally, the products were calcinated at 300 °C for 6 h in the tubular furnace under argon flow. The bamboo-based activated carbon and bamboo-based activated carbon @ MnO<sub>2</sub> nanocomposites obtained at different time ( 60, 90, 120 min ) are abbreviated to BC, BCMNc-60, BCMNc-90 and BCMNc-120, respectively.

The weight percentage of MnO<sub>2</sub> in each sample was estimated by thermogravimetric curve. The MnO<sub>2</sub> was transformed into Mn<sub>3</sub>O<sub>4</sub> from 25 to 900 °C in the air [24]. According to the law of conservation of mass and the law of conservation of elements, the mass and weight percentage of MnO<sub>2</sub> in each nanocomposite could be calculated. The mass of MnO<sub>2</sub> on the working electrodes could be obtained according to this weight percentage.

## 2.2 Material and electrode characterization

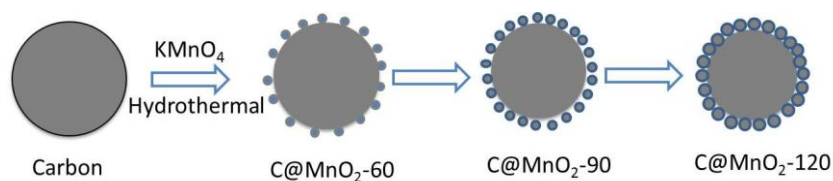
X-ray diffraction patterns were recorded on a DX-2700 diffractometer (China) using copper  $K\alpha$  radiation ( $\lambda=1.5418\text{\AA}$ ). Scanning electron microscopy (SEM) images were obtained using a JEOL JSM-6700 FE-SEM.

The electrodes were assembled on nickel foam collectors. Briefly, 85 wt.% of the electroactive material, 10 wt.% of carbon black, and 5 wt.% of poly (tetrafluoroethylene) were mixed to form a slurry. The slurry was rolled into thin slice by the glass rod, then thin slice was coated on a nickel foam substrate to make electrodes. Finally, the prepared electrodes were subjected to a pressure of 3 MPa and then dried at  $80^\circ\text{C}$  for 12 h under vacuum.

Electrochemical measurements were performed in a solution of 1 M  $\text{Na}_2\text{SO}_4$  aqueous electrolyte using a three-electrode cell. A platinum plate and a saturated calomel electrode were used as counter and reference electrodes, respectively. The mass of electroactive materials (BC, BCMNc-60, BCMNc-90 and BCMNc-120) were used to make working electrodes. Cyclic voltammetry (CV) was carried out using an electrochemical working station (CHI660D, Shanghai, China) at room temperature. Cycle voltammetry (CV) measurements were performed in the voltage between 0 and 0.6 V at different scan rates. Cycling stability test was carried out using a high-precision battery testing system (NEWARE BTS, Shenzhen, China) at room temperature.

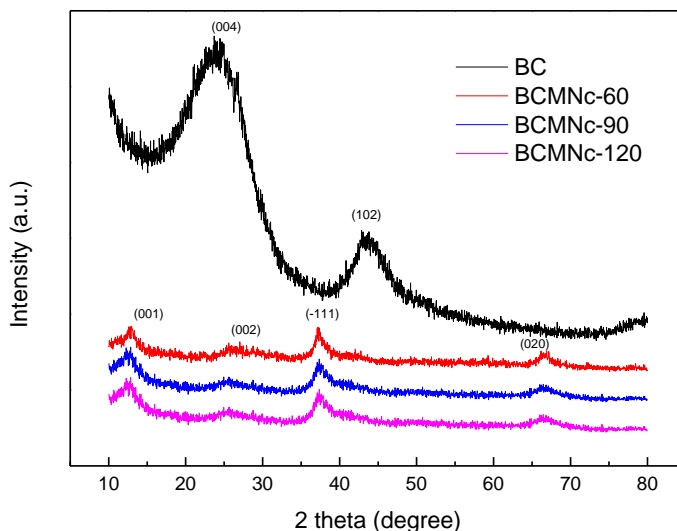
## 3. RESULTS AND DISCUSSION

### 3.1 Structure and surface morphology characterization



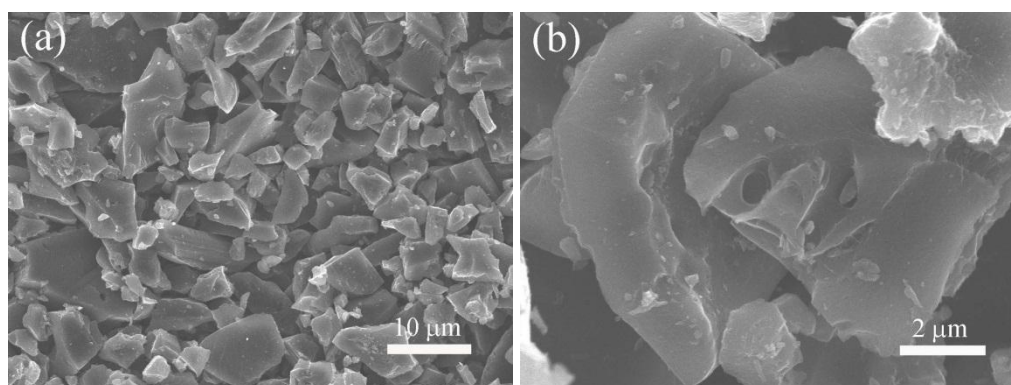
**Figure 1.** Schematic illustration of the fabrication process of the nanocomposites

The hybrid bamboo-based activated carbon@ $\text{MnO}_2$  nanocomposites (BCMNC for short) were synthesized by one step hydrothermal method. Fig.1 illustrates a representative fabrication process of the BCMNC. Specifically,  $\text{MnO}_2$  shells were nucleated and grown on the surfaces of the bamboo-based activated carbon. The structure, composition and interfaces of nanocomposites depended on temperature and time of reaction. The particle sizes of  $\text{MnO}_2$  get bigger with the increasing reaction time. Herein we prepared the nanocomposites at  $100^\circ\text{C}$  for 60, 90 and 120 minutes. The weight percentage of  $\text{MnO}_2$  in the BCMNC-60, BCMNC-90 and BCMNC-120 were 28.61%, 51.57% and 58.39%, respectively, which were estimated by thermogravimetric curves.



**Figure 2.** The X-ray diffraction of four samples

The crystal phase and structure information were obtained by XRD measurements. The XRD pattern was identified by comparison with the JCPD standard. The crystalline size  $D_c$  was determined by using the Scherrer equation,  $D_c = 0.89\lambda / (B \cos\theta)$ , where  $\lambda$  is the corrected wavelength of the X-radiation,  $B$  is the full width at half-maximum corrected for instrumental broadening, and  $\theta$  is the Bragg angle of the diffraction peak. As shown in Fig.2, the diffractive curve of BC is different from the diffractive curves of BCMNc-60, BCMNc-90 and BCMNc-120. The diffraction peaks at 2 theta of 23.13 and 44.28 can be indexed as (004) and (102) crystal planes of bamboo-based activated carbon. The diffractive curves of BCMNc-60, BCMNc-90 and BCMNc-120 are similar. The diffraction peaks at 2 theta of 12.64, 25.60, 37.19 and 66.90 can be indexed as (001), (002), (-111) and (020) crystal planes, which corroborate well with the standard XRD pattern of birnessite-type manganese oxide crystal ( JCPDS 80-1098,  $a=5.149 \text{ \AA}$ ,  $b=2.843 \text{ \AA}$ ,  $c=7.716 \text{ \AA}$  ) [25]. It also can be calculated that the average grain size of nanocomposites by applying Scherrer's equation. The mean grain sizes are about 14.38 nm, 16.92 nm and 27.61 nm for the BCMNc-60, BCMNc-90 and BCMNc-120, respectively. It's obvious that the particle sizes of  $MnO_2$  get bigger with the increasing reaction time.



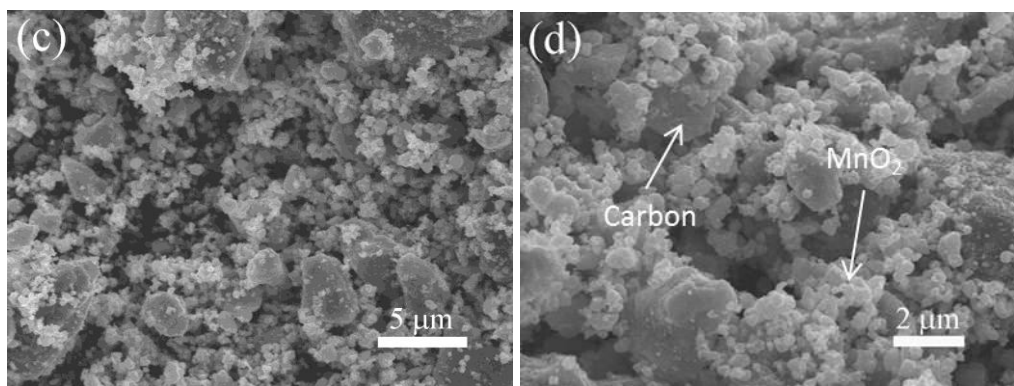
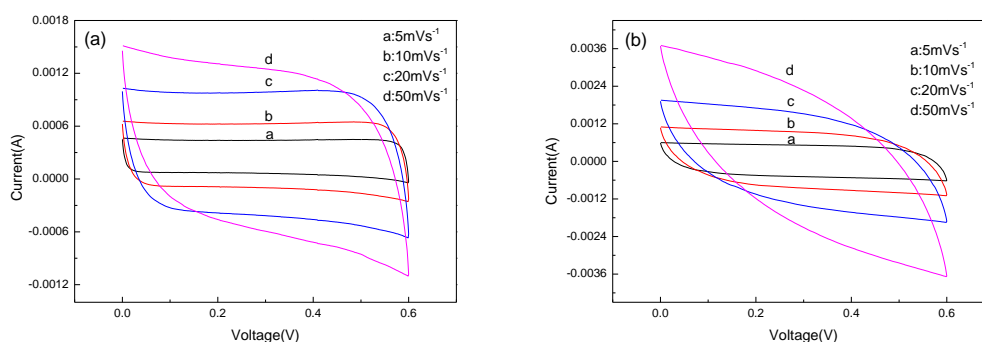


**Figure 3.** (a), (b) SEM images of BC at different magnification; (c), (d) SEM images of BCMNc-90 at different magnification.

The morphologies and structures of these bamboo-based activated carbon @ MnO<sub>2</sub> nanocomposites can be further investigated by SEM. The typical SEM images of bare bamboo-based activated carbon at different magnification are shown in Fig.3(a)-(b). It can be seen that the bamboo-based activated carbons with smooth surfaces had a size range from about 90 to 500 nm, and they had large junked irregular pieces distributed randomly, which looked like small broken rocks at 2000 times magnification (see Fig.3(a)). However, after reacting with KMnO<sub>4</sub>, the bamboo-based activated carbons had been turned into relatively uniform and small fragments, MnO<sub>2</sub> nanoshells were observed to form and anchor on the surfaces of the bamboo-based activated carbons (see Fig.3(c)-(d)). The MnO<sub>2</sub> nanoshells were interconnected each other, forming a highly porous surface morphology (see Fig.3(c)-(d)). Porous morphology was crucial to energy storage performances. The conductive network by in situ formation of manganese dioxide on the surfaces of bamboo-based activated carbons could increase the electrical contact with the current collector, which resulted in better charge transfer kinetics and an enhanceive electrochemical capacity [25].

### 3.2 Capacitive performance of nanocomposites

The electrochemical performances of the BCMNc as electrode materials were investigated in a three-electrode system using 1.0 M Na<sub>2</sub>SO<sub>4</sub> solution as electrolyte.



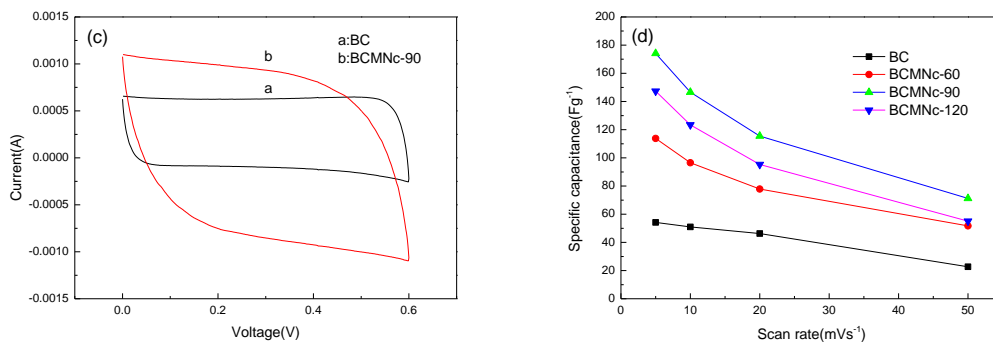


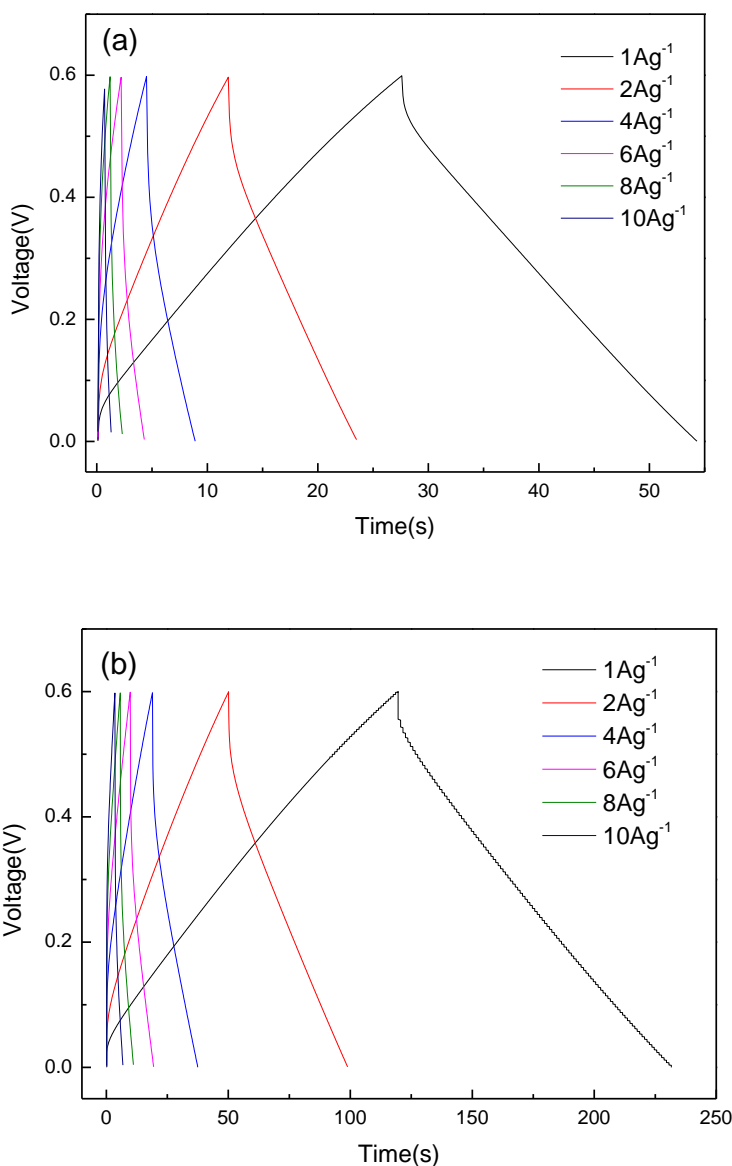
**Figure 4.** (a) Cyclic voltammetry curves of BC at different scan rates from 5 to 50 mV s<sup>-1</sup>; (b) cyclic voltammetry curves of BCMNc-90 at different scan rates from 5 to 50 mV s<sup>-1</sup>; (c) cyclic voltammetry curves of BC and BCMNc-90 at 10 mV s<sup>-1</sup> scan rate; (d) calculated specific capacitance of the BC, BCMNc-60, BCMNc-90 and BCMNc-120 samples as a function of the scan rate.

CV measurements and galvanostatic charge-discharge test have been performed to evaluate the electrochemical properties and quantify the specific capacitance of the as-prepared nanocomposite electrodes. Fig.4a presents the cyclic voltammogram (CV) curves of the BC sample. It is found that all the CV curves share a similar shape and the current increases with the increasing scan rates from 5, 10, 20 and 50 mV s<sup>-1</sup>. The very symmetric rectangular shape is obviously observed during the anodic and cathodic sweeps of the CV curves in all scan rates, which clearly reveals the ideal electrical double-layer capacitive characteristic of the sample. The rectangular shape can be attributed to the adsorption and desorption of electrolyte ions within BC, and the redox reaction wouldn't take place on the surfaces of the BC [3]. However, after reacting with KMnO<sub>4</sub>, the CV curves of the BC have changed. As shown in Fig.4b, it can be seen clearly that the current increases with increasing the scan rates from 5, 10, 20 and 50 mV s<sup>-1</sup> and the CV curve of the BCMNc-90 is a near rectangular with symmetrical feature, implying the electrical double-layer capacitive behavior and a typical character of reversible redox reaction of the electrode active materials. Even at the high scan rate of 50 mV s<sup>-1</sup> the CV curve can still keep nearly rectangular and symmetrical shape, indicating the excellent electrochemical activity and high reversibility of the BCMNc-90 electrode. In order to further distinguish between the CV curve of the BC and BCMNc-90, they were put together in one figure at the same scan rate. Fig.4c shows the cyclic voltammetry (CV) curves of the BC and BCMNc-90 at the same scan rate of 10 mV s<sup>-1</sup> with a potential window from 0 to 0.6 V. It can be seen clearly that the shape of CV curve of the BCMNc-90 is symmetric, sharp and near rectangular, which is different from the shape of CV curve of the BC. Furthermore, the area covered by the CV curve of the BCMNc-90 is bigger than that of the BC, indicating the excellent electrochemical activity and high specific capacitance of the BCMNc-90 electrode.

The average specific capacitance of the nanocomposite electrodes can be calculated from the CV curves by integrating the area under the current-potential curve:

$$C = \frac{1}{s \cdot m \cdot \Delta V} \int_{V_2}^{V_1+\Delta V} I(V) dV$$

where  $I(A)$  is the current,  $m(g)$  is the mass of the active material in the electrode,  $s(V s^{-1})$  is the scan rate,  $V$  is the voltage in the CV curve. Fig.4d shows the average specific capacitances of the BC and the three BCMNc at various scan rates. Obviously, the average specific capacitances exhibit a decreasing tendency from the BC, BCMNc-60, BCMNc-90 to BCMNc-120 with the increased scan rate. Among them, the BCMNc-90 shows the best capacitive performance. Based on the CV curves, the average specific capacitance of BCMNc-90 is calculated to be 174.11, 146.63, 115.44, 71.19  $F g^{-1}$  at the scan rates of 5, 10, 20 and 50  $mV s^{-1}$ , respectively. However, the average specific capacitance of BC is calculated to be 54.15, 50.98, 46.26, 22.68  $F g^{-1}$  at the scan rates of 5, 10, 20 and 50  $mV s^{-1}$ , respectively. The huge increase of capacitance is attributed to the presence of  $MnO_2$  grown on the surface of the bamboo-based activated carbon which is able to generate the redox reaction. Moreover, the BCMNc-90 electrode also shows an excellent rate capability. Its average specific capacitance can still reach 71.19  $F g^{-1}$  even at a high scan rate of 50  $mV s^{-1}$ .



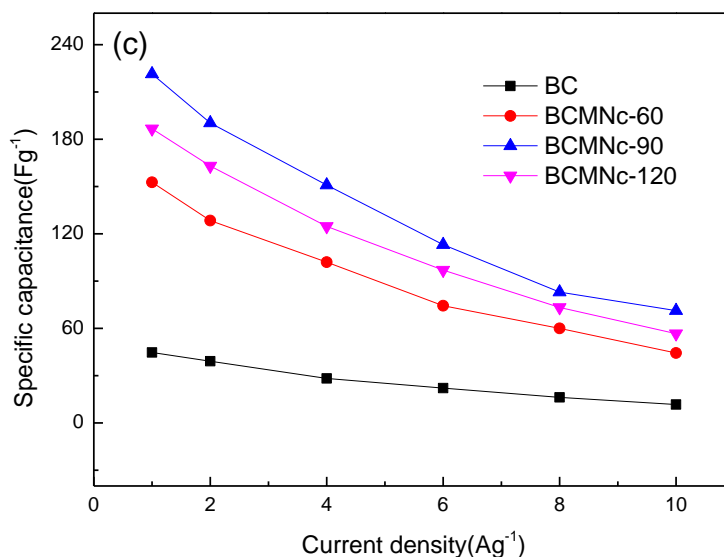


**Figure 5.** (a) Galvanostatic charge/discharge curves with different current densities for the BC electrode; (b) galvanostatic charge/discharge curves with different current densities for the BCMNc-90 electrode; (c) calculated specific capacitance of the BC, BCMNc-60, BCMNc-90 and BCMNc-120 samples with different current densities.

To further confirm the excellent capacitance performances and evaluate the potential application of the bamboo-based activated carbon @ MnO<sub>2</sub> sample, galvanostatic charge-discharge (GCD) measurement was also conducted in 1 M Na<sub>2</sub>SO<sub>4</sub> solution with the currents ranging from 1 to 10 A g<sup>-1</sup>. Fig.5a and b show the constant current charge-discharge profiles of the BC and BCMNc-90 at different current densities. It can be observed that all the potential-time curves are nearly symmetric, indicating the high coulombic efficiency under various current densities, and the slope of every part in each pair is nearly a constant, which also indirectly prove the ideal capacitive behaviors for the supercapacitors. But the BCMNc-90 exhibited relative bigger integrated area and longer discharge time than the BC. The specific capacitance of the curves can be calculated according to the following equation:

$$C_m = \frac{C}{m} = \frac{I \times \Delta t}{\Delta V \times m}$$

where,  $C_m$  (F g<sup>-1</sup>) is the specific capacitance,  $I$  (A) is discharge current,  $\Delta t$  (s) is the discharging time,  $\Delta V$  (V) represents the potential drop during discharge process, and  $m$  (g) is the mass of the active material in the electrode. The calculated specific capacitance as a function of the discharge current density is plotted in Fig.5c. The specific capacitances of BC are 44.67, 39.17, 28.24, 22.13, 16.21 and 11.67 F g<sup>-1</sup> at different current densities of 1, 2, 4, 6, 8 and 10 A g<sup>-1</sup>, respectively. However, the specific capacitances of BCMNc-90 are 221.45, 190.37, 150.89, 113.07, 82.99 and 71.23 F g<sup>-1</sup> at different current densities of 1, 2, 4, 6, 8 and 10 A g<sup>-1</sup>, respectively, indicating better electrochemical performance. Such excellent specific capacitances of the BCMNc-90 may be ascribed to its synergistic effect of two component [8]. Therein bamboo-based activated carbon has an extraordinarily porous 3D

microstructure and high absorptive capacity. Moreover,  $\text{MnO}_2$ 's particle size is about 16.92nm according to the Scherrer equation, its specific area is big. Therefore, there are many redox reaction sites on the surfaces of  $\text{MnO}_2$ .

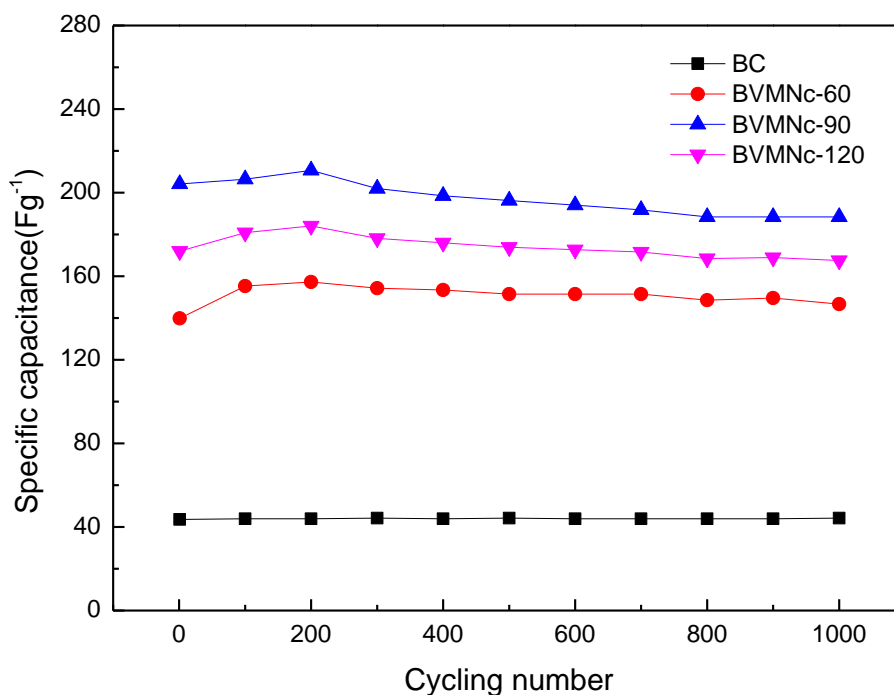


**Figure 6.** Cycle performance of the electrodes during 1000 cycles at the current density of  $1 \text{ A g}^{-1}$

In practice, long cycle life is a prerequisite requirement for electrode materials. Hence, the cycling stability of BC, BCMNc-60, BCMNc-90 and BCMNc-120 were performed by charge-discharge test at a current density of  $1 \text{ A g}^{-1}$ . As shown in Fig.6, the specific capacitance of BCMNc-90 has a gradual increase in the second hundred cycles, and can reach a maximum value of  $210.96 \text{ F g}^{-1}$ . Then it decreases slightly compared with the maximum value. And the specific capacitance of BCMNc-90 still remained  $188.36 \text{ F g}^{-1}$ , and degraded only by 10.71% after 1000 cycles of charge-discharge. A similar phenomenon was also showed in Fig.6 for the BCMNc-60 and BCMNc-120. As for the BC, the curve of specific capacitance is almost a horizontal line. Almost 99.98% of initial value is retained after 1000 cycles, indicating its excellent cycling stability. Although the BC has its excellent cycling stability, the specific capacitance of BC is only  $43.60 \text{ F g}^{-1}$  at a current density of  $1 \text{ A g}^{-1}$ , which is lowest among them.

All of the measurement results mentioned above show the obvious differences of electrochemical performance of the BC, BCMNc-60, BCMNc-90 and BCMNc-120. These can be ascribed to the difference of their morphology, structure, composition and interfaces. It is clear that these three kinds of BCMNc have better electrochemical performance than the BC. Moreover, the electrochemical performances are similar for the BCMNc-60, BCMNc-90 and BCMNc-120. Among

them, the BCMNc-90 has the best electrochemical performances. The reasons may be attributed the following explanations. Firstly, the BCMNc-90 has a uniform core-shell structure with MnO<sub>2</sub> anchored closely to the surface of bamboo-based activated carbon, which can provide effective charge-transport routes. Although the mean grain size of the BCMNc-60 is about 14.38 nm and smaller than the BCMNc-90's, the weight percentage of MnO<sub>2</sub> in the BCMNc-60 is 28.61% and lower than the weight percentage of MnO<sub>2</sub> in the BCMNc-90. Although the weight percentage of MnO<sub>2</sub> in the BCMNc-120 is 58.39% and higher than the weight percentage of MnO<sub>2</sub> in the BCMNc-90, the mean grain size of the BCMNc-120 is about 26.71 nm and higher than the BCMNc-90's. Secondly, the appropriate thickness of MnO<sub>2</sub> nanoparticles on the surfaces of the bamboo-based activated carbon can maximize the utilization of active material, shorten the ion transport path and improve the intercalation of ions at the interface between active material and electrolyte [16].

#### 4. CONCLUSIONS

In summary, a facile, low-cost and practical approach has been developed to fabricate the bamboo-based activated carbon @ MnO<sub>2</sub> nanocomposites which can be used as supercapacitor electrode materials. By simply controlling the reaction time, three kinds of nanocomposites (BCMNC-60,-90 and -120) with different composition ratio and structure have been prepared. Electrochemical measurements show that the BCMNc-90 exhibits the best electrochemical performances: a high specific capacitance of 174.11 F g<sup>-1</sup> at the scan rate of 5 mV s<sup>-1</sup>, a high specific capacitance of 221.45 F g<sup>-1</sup> at the current density of 1 A g<sup>-1</sup> and a good cycling performance with 89.29% retention after 1000 cycles at the current density of 1 A g<sup>-1</sup> can be reached. Considering the low cost, efficiency and easy control of this synthesis process, and the good electrochemical performances of the products, these bamboo-based activated carbon @ MnO<sub>2</sub> nanocomposites have a great potential in commercial application.

#### ACKNOWLEDGEMENT

This work was financially supported by the Science and Technology Key Project of Fujian Province (2014H0038), the Science and Technology Program of LongYan (2014LY36) and the School Research Program of LongYan University (LC2013008).

#### References

1. C. H. An, Y. J. Wang, Y. A. Huang, Y. N. Xu, C. C. Xu, L. F. Jiao, H. T. Yuan, *CrystEngComm.*, 16 (2014) 385.
2. Y. M. Wang, J. C. Chen, J. Y. Cao, Y. Liu, Y. Zhou, J. H. Ouyang, D. C. Jia, *J. Power Sources*, 71 (2014) 269.
3. S. Faraji, F. N. Ani, *Renew. Sust. Energ. Rev.*, 42 (2015) 823.
4. H. C. Youn, S. H. Park, K. C. Roh, K. B. Kim, *Curr. Appl. Phys.*, <http://dx.doi:10.1016/j.cap.2015.01.031>.

5. Y. Li, H. Q. Xie, J. F. Wang, L. F. Chen, *Mater. Lett.*, 65 (2011) 403.
6. G. A. Snook, P. Kao, A. S. Best, *J. Power Sources*, 196 (2011) 1.
7. Z. x. Song, Y. J. Zhang, W. Liu, S. Zhang, G. C. Liu, H. Y. Chen, J. S. Qiu, *Electrochim. Acta*, 112 (2013) 120.
8. D. Eder, *Chem. Rev.*, 110 (2010) 1348.
9. S. H. Li, Q. H. Liu, Q. Li, L. H. Lu, H. Y. Wang, *Chin. J. Anal. Chem.*, 40 (2012) 339.
10. K. J. Huang, J. Z. Zhang, K. Xing, *Electrochim. Acta*, 149 (2014) 28.
11. T. M. Dinh, A. Achour, S. Vizireanu, G. Dinescu, L. Nistor, K. Armstrong, D. Guay, D. Pech, *Nano Energy*, 10 (2014) 288.
12. S. Vijayakumar, S. Nagamuthu, G. Muralidharan, *ACS Appl. Mater. Interfaces*, 5 (2013) 2188.
13. T. C. Liu, W. G. Pell, B. E. Conway, *Electrochim. Acta*, 42 (1997) 3541.
14. A. G. Xiao, S. B. Zhou, C. G. Zuo, Y. B. Zhuan, X. Ding, *Mater. Res. Bull.*, 60 (2014) 674.
15. K. Y. Liu, Y. Zhang, W. Zhang, H. Zheng, G. Su, *Trans. Nonfer. Met. Soc. Chin.*, 17 (2007) 649.
16. Y. Zhao, Y. N. Meng, P. Jiang, *J. Power Sources*, 259 (2014) 219.
17. Y. T. Peng, Z. Chen, J. Wen, Q. F. Xiao, D. Weng, S. Y. He, H. B. Geng, Y. F. Lu, *Nano Res.*, 4 (2011) 216.
18. S. Zhu, H. Zhou, M. Hibino, I. Honma, M. Ichihara, *Adv. Funct. Mater.*, 15 (2005) 381.
19. Y. J. Li, G. L. Wang, K. Ye, K. Cheng, Y. Pan, P. Yan, J. L. Yin, D. X. Cao, *J. Power Sources*, 271 (2014) 582.
20. C. Y. Guo, H. Li, X. Zhang, H. H. Huo, C. L. Xu, *Sensor. Actuat. B. Chem.*, 206 (2015) 407.
21. A. E. Fischer, K. A. Pettigrew, D. R. Rolison, R. M. Stroud, J. W. Long, *Nano. Lett.*, 7 (2007) 281.
22. G. R. Li, Z. P. Feng, Y. N. Ou, D. C. Wu, R. W. Fu, Y. X. Tong, *Langmuir*, 26 (2010) 2209.
23. C. S. Yang, Y. S. Jang, H. K. Jeong, *Curr. Appl. Phys.*, 14 (2014) 1616.
24. X. X. Zhang, F. Ran, H. L. Fan, L. B. Kong, L. Kang, *Acta Phys. Chim. Sin.*, 30 (2014) 881.
25. S. J. Zhu, W. L. Cen, L. L. Hao, J. J. Ma, L. Yu, H. L. Zheng, Y. X. Zhang, *Mater. Lett.*, 135 (2014) 11.